

# Analysis of local buckling in steel Square and Rectangular Hollow Section via Lumped Damage Mechanics

Leonardo A. B. Silva<sup>1</sup>, Higor S. D. de Argôlo<sup>2</sup>, David L. N. F. Amorim<sup>1,2</sup>

<sup>1</sup>Post-graduate Programme in Civil Engineering, Federal University of Alagoas  
Av. Lourival Melo Mota s/n, Tabuleiro do Martins, 57072-970, Maceió/AL, Brazil  
leonardo.bispo@ctec.ufal.br

<sup>2</sup>Disaster Research Institute, Department of Civil Engineering, Federal University of Sergipe  
Av. Marcelo Deda Chagas s/n, Rosa Elze, 49107-230, São Cristóvão/SE, Brazil  
higorsergio@academico.ufs.br, davidnf@academico.ufs.br

**Abstract.** This paper presents a lumped damage model to analyse local buckling in steel Square (SHS) and Rectangular Hollow Section (RHS). In this model, the nonlinear and damage effects of the planar frame element are concentrated in plastic hinges located at the ends of the element, significantly reducing the computational cost of the analysis. Thus, plasticity effects are represented by the formation of plastic hinges, while local buckling is described by adding a damage variable to these hinges. The analysis adopts a step-by-step procedure to consider geometric nonlinearity, solving the problem sequentially, and considering the structural elements' geometry change. To evaluate the model's accuracy, the numerical results were compared with experimental results, in which steel SHS were subjected to compressive axial force with monotonic bending moment loading. The results indicate that the numerical model presents satisfactory behaviour in relation to the experimental results.

**Keywords:** local buckling, square hollow section, rectangular hollow section, lumped damage mechanics.

## 1 Introduction

Square (SHS) and rectangular hollow section (RHS) columns are widely used in steel building construction, especially in regions subject to seismic activity, due to their strength and rigidity in both directions. However, during high-magnitude earthquakes, local buckling may occur in these columns, potentially leading to the collapse of the entire structure [1]. Thus, several studies have been developed to understand and describe the local buckling behaviour in steel SHS and RHS [2-6].

Among the various numerical methods available, Lumped Damage Mechanics (LDM) stands out for its simplified implementation and computational efficiency. In this method, it is assumed that all nonlinear and damage effects of a finite element are lumped in inelastic hinges at the ends of the element. This approach significantly reduces the computational cost of the analysis, allowing its application in reliability analyses [7-8] and in several practical engineering problems, such as local buckling [9-13].

Thus, the main objective of this paper is to present a geometrically nonlinear lumped damage model to analyse local buckling in steel square and rectangular hollow sections.

## 2 Lumped damage mechanics

Consider a planar frame element  $b$  between nodes  $i$  and  $j$ , as illustrated in Fig. 1a. The element has six degrees of freedom: horizontal and vertical displacements, and rotations at each node ( $u$ ,  $w$  and  $\theta$ , respectively).

Thus, the matrix of generalised displacements of the finite element is defined as:

$$\{\mathbf{q}\}_b = \{u_i \quad w_i \quad \theta_i \quad u_j \quad w_j \quad \theta_j\}^T \quad (1)$$

where the superscript  $T$  means ‘transpose of’.

Analogously, the matrix of internal forces of the element  $b$  is given by:

$$\{\mathbf{Q}\}_b = \{Q_{ui} \quad Q_{wi} \quad Q_{\theta i} \quad Q_{uj} \quad Q_{wj} \quad Q_{\theta j}\}^T \quad (2)$$

where the first index means the direction and the second one is the node where it is applied, e.g.  $Q_{wj}$  is the internal force at the  $Z_G$ -axis direction applied on node  $j$ .

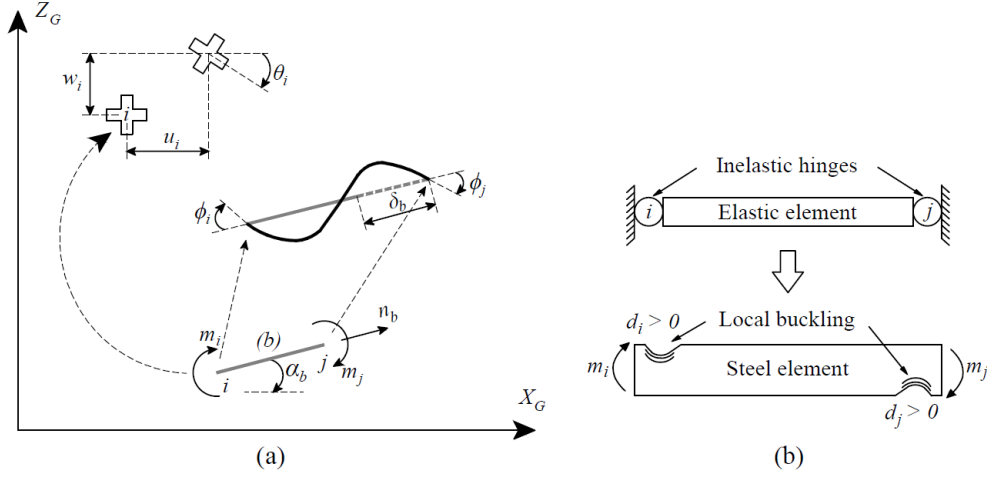


Figure 1. Planar frame element: (a) generalised displacements and deformations and (b) lumped damage model for steel

The notation used in this paper is based on the one proposed by Powell [14], where the rigid body movement is separated from the frame deformation. Thus, the deformed shape of the element  $b$  can be described by the matrix of generalised deformations:

$$\{\boldsymbol{\phi}\}_b = \{\phi_i \quad \phi_j \quad \delta_b\}^T \quad (3)$$

where  $\phi_i$  and  $\phi_j$  are the relative rotations at the respective nodes, and  $\delta_b$  is the elongation of the element (Fig. 1a).

The matrix of generalised deformations is conjugated to the matrix of generalised stresses, given by:

$$\{\boldsymbol{\sigma}\}_b = \{m_i \quad m_j \quad n_b\}^T \quad (4)$$

where  $m_i$  and  $m_j$  are the bending moments at the respective nodes, and  $n_b$  is the axial force (Fig. 1a).

The relation between displacements and generalised deformations of the finite element is established by the kinematic equation, described by:

$$\{d\boldsymbol{\phi}\}_b = [\mathbf{B}(\mathbf{q})]_b \{d\mathbf{q}\}_b \quad (5)$$

where  $[\mathbf{B}(\mathbf{q})]_b$  is the kinematic transformation matrix [15], expressed by:

$$[\mathbf{B}(\mathbf{q})]_b = \begin{bmatrix} \frac{\sin \alpha_b}{L_b} & -\frac{\cos \alpha_b}{L_b} & 1 & -\frac{\sin \alpha_b}{L_b} & \frac{\cos \alpha_b}{L_b} & 0 \\ \frac{\sin \alpha_b}{L_b} & -\frac{\cos \alpha_b}{L_b} & 0 & -\frac{\sin \alpha_b}{L_b} & \frac{\cos \alpha_b}{L_b} & 1 \\ -\cos \alpha_b & -\sin \alpha_b & 0 & \cos \alpha_b & \sin \alpha_b & 0 \end{bmatrix} \quad (6)$$

being  $\alpha_b$  the angle of inclination between the axis of the finite element and the reference coordinate system and  $L_b$  is the current length of the element.

Thus, the matrix of internal forces can be related to the matrix of generalised stresses as follows:

$$\{\mathbf{Q}\}_b = [\mathbf{B}(\mathbf{q})]_b^T \{\boldsymbol{\sigma}\}_b \quad (7)$$

In LDM, the damage variable is incorporated into plastic hinges, which are generically called inelastic hinges. It is assumed that the plasticisation of the steel structure and discontinuity due to local buckling are concentrated at the ends of the element. Thus, the plasticisation of the structural element is represented by forming a plastic hinge. In contrast, the local buckling at the end of the element is described by the damage variables ( $d_i$  and  $d_j$ ) added to the hinges, as illustrated in Fig. 1b.

According to the deformation equivalence hypothesis [15], the matrix of generalised deformations can be expressed as:

$$\{\boldsymbol{\phi}\} = \{\boldsymbol{\phi}^e\} + \{\boldsymbol{\phi}^p\} + \{\boldsymbol{\phi}^d\} \quad (8)$$

where  $\{\boldsymbol{\phi}^e\}$  is the elastic part of the matrix of generalised deformations,  $\{\boldsymbol{\phi}^p\}$  is the matrix of plastic generalised deformations, and  $\{\boldsymbol{\phi}^d\}$  is the part due to damage. Considering that plastic elongations can be neglected, the matrix of plastic generalised deformations is given by:

$$\{\boldsymbol{\phi}^p\} = \{\phi_i^p \quad \phi_j^p \quad 0\}^T \quad (9)$$

Thus, the constitutive law relates the matrix of generalised deformations  $\{\boldsymbol{\phi}\}_b$  to the matrix of generalised stresses  $\{\boldsymbol{\sigma}\}_b$  as follows:

$$\{\boldsymbol{\phi} - \boldsymbol{\phi}^p\}_b = [\mathbf{F}(d)]_b \{\boldsymbol{\sigma}\}_b \quad (10)$$

where  $[\mathbf{F}(d)]_b$  is the flexibility matrix of the damaged frame element [15], described by:

$$[\mathbf{F}(d)]_b = \begin{bmatrix} \frac{L_b}{3EI_b(1-d_i)} & -\frac{L_b}{6EI_b} & 0 \\ -\frac{L_b}{6EI_b} & \frac{L_b}{3EI_b(1-d_j)} & 0 \\ 0 & 0 & \frac{L_b}{EA_b} \end{bmatrix} \quad (11)$$

where  $EI_b$  and  $EA_b$  are, respectively, the flexural (Young's modulus multiplied by moment of inertia of the cross-section) and axial (Young's modulus multiplied by the area of the cross-section) rigidities.

The analysis was performed sequentially to consider the nonlinear effects due to the change in the geometry of the structural elements. Thus, the kinematic, equilibrium and constitutive equations were formulated using the same variables but expressed as a function of time, i.e.  $\{\mathbf{q}\} = \{\mathbf{q}(t)\}$ ;  $\{\boldsymbol{\phi}\} = \{\boldsymbol{\phi}(t)\}$ ;  $\{\mathbf{Q}\} = \{\mathbf{Q}(t)\}$ ;  $\{\boldsymbol{\sigma}\} = \{\boldsymbol{\sigma}(t)\}$  for  $0 \leq t \leq T$ . Therefore, the kinematic equation can be rewritten as:

$$\{\boldsymbol{\phi} - \boldsymbol{\phi}_{t-1}\}_b = [\mathbf{B}(\mathbf{q}_{t-1})]_b \{\mathbf{q}_t - \mathbf{q}_{t-1}\}_b \quad (12)$$

The nonlinear behaviour of the elastic-plastic regime was described using the following relations as yield functions for the inelastic hinges  $i$  and  $j$ :

$$\begin{aligned} f_i(m_i, n) &= \frac{|m_i|}{(1-d_i)M_y} + \frac{|n|}{N_y} - 1 - \frac{1}{M_y} [M_u(n) - M_y(n)] [1 - \exp(-\beta\phi_i^p)] \leq 0; \\ f_j(m_j, n) &= \frac{|m_j|}{(1-d_j)M_y} + \frac{|n|}{N_y} - 1 - \frac{1}{M_y} [M_u(n) - M_y(n)] [1 - \exp(-\beta\phi_j^p)] \leq 0 \end{aligned} \quad (13)$$

where  $\beta$  is a material constant,  $M_y(n) = (1 - |n|/N_y)M_y$  and  $M_u(n) = (1 - (|n|/N_y)^2)M_u$ .

Thus, the plastic evolution laws for both hinges are given by:

$$\begin{cases} d\phi^p = 0 & \text{if } f_i(m_i, n) < 0 \text{ (hinge } i \text{ is locked)} \\ f_i(m_i, n) = 0 & \text{if } d\phi^p \neq 0 \text{ (hinge } i \text{ is active)} \end{cases} \quad (14)$$

$$\begin{cases} d\phi_j^p = 0 & \text{if } f_j(m_j, n) < 0 \text{ (hinge } j \text{ is locked)} \\ f_j(m_j, n) = 0 & \text{if } d\phi_j^p \neq 0 \text{ (hinge } j \text{ is active)} \end{cases}$$

Since the damage variable was introduced into the constitutive law and yield functions with local buckling, it is necessary to insert a new equation into the model, called the damage evolution law, which numerically establishes the evolution of local buckling, represented by the damage variable. This paper adopts the following damage evolution law for ductile materials [16], which has also been applied in the analyses via LDM performed by [9-10, 12-13]:

$$d_i = k_m \langle \phi_i^p - p_{cri} \rangle_+ \quad (15)$$

where  $p_{cri}$  is the critical plastic rotation that initiates the local buckling,  $k_m$  is the slope of the damage evolution line and  $\langle \rangle_+$  indicates that only values greater than zero are taken. The parameters  $p_{cri}$  and  $k_m$  can be obtained experimentally.

To estimate the value of the parameter  $p_{cr}$  without the need for experiments, this paper used the following expression based on the stress and strain distributions in a cross-section:

$$p_{cr} = \left( \frac{\varepsilon_u}{z_{NAu}} - \frac{\varepsilon_y}{z_{NAy}} \right) L_p \quad (16)$$

where  $\varepsilon_y$  is the elastic limit strain,  $\varepsilon_u$  is the ultimate strain,  $z_{NAy}$  is the neutral axis in the elastic limit,  $z_{NAu}$  is the neutral axis associated with the ultimate strength stress, and  $L_p$  is the plastic hinge length, which represents the length of the zone of the element that is subject to plastic deformations.

The ultimate strain  $\varepsilon_u$  for SHS and RHS can be determined using the following equation [17]:

$$\varepsilon_u = \mu_0 \varepsilon_y \quad (17)$$

where the strain ductility factor ( $\mu_0$ ) can be determined as [17]:

$$\mu_0 = 8.7/\alpha - 1.2 \quad (0.19 \leq 1/\alpha \leq 2.62) \quad (18)$$

$$\alpha = \varepsilon_y (b/t)^2 \quad (19)$$

being  $b$  and  $t$  the width and thickness of the cross-section, respectively.

### 3 Results

To evaluate the performance of the lumped damage model, numerical simulations were performed to compare the results obtained with the experiments carried out by Kazuya [18]. The experimental campaign was conducted with the aim of investigating the resistance capacity and deformation properties of SHS subjected to axial compression and monotonic bending moment. Table 1 presents the values of Young's modulus ( $E$ ), yield stress ( $f_y$ ), width ( $b$ ), thickness ( $t$ ), area ( $A$ ), moment of inertia ( $I$ ), plastic section modulus ( $Z_p$ ) and plastic moment ( $M_p$ ) of the SHS 125x125x6 mm and 150x150x9 mm used in the experiments.

Table 1. Mechanical properties and geometric dimensions of cross-sections. Adapted from Kazuya [18]

Cross-section	$E$ (N/mm <sup>2</sup> )	$f_y$ (N/mm <sup>2</sup> )	$b$ (mm)	$t$ (mm)	$A$ (mm <sup>2</sup> )	$I$ (x 10 <sup>4</sup> mm <sup>4</sup> )	$Z_p$ (x 10 <sup>3</sup> mm <sup>3</sup> )	$M_p$ (kN.m)
125x125x6	201800	405.2	125.0	5.827	2707	632.4	119.9	48.58
150x150x9	211200	386.7	150.2	8.667	4713	1540	246.5	95.32

According to the ANSI/AISC 360-22 [19], the cross-sections 125x125x6 mm and 150x150x9 are classified as compact for the flexural design of SHS. Thus, it is considered that the nominal flexural strength is equal to the plastic moment ( $M_p$ ). However, this approach may result in more conservative estimates of the ultimate moment ( $M_u$ ), as it neglects the additional resistance capacity due to hardening, which may occur before local buckling. Tayyebi et al. [20] experimentally investigated the behaviour of SHS and RHS under bending conducting tests on twenty-two specimens, eleven of which were compact sections. For these compact sections, the estimates of flexural strength based on plastic moments were conservative, with an average ratio between experimental ultimate moments and plastic moments of 1.20. Therefore, considering that equality between the ultimate moment and plastic moment can lead to conservative predictions, this paper performed numerical simulations adopting  $M_u = 1.20M_p$ .

In Kazuya's experiments [18], an axial compression force was applied using a hydraulic jack positioned on the west side of the specimen. Simultaneously, a monotonic bending moment was applied on the east side of the specimen using the binary force generated by auxiliary bars, as shown in Fig. 2. The value of the bending moment was determined by multiplying the binary force by the distance between the bar and the rotation axis. The load on the auxiliary bars was applied until the specimen could no longer support the compression force or until reaching the maximum rotation of the experiment, approximately 0.30 rad.

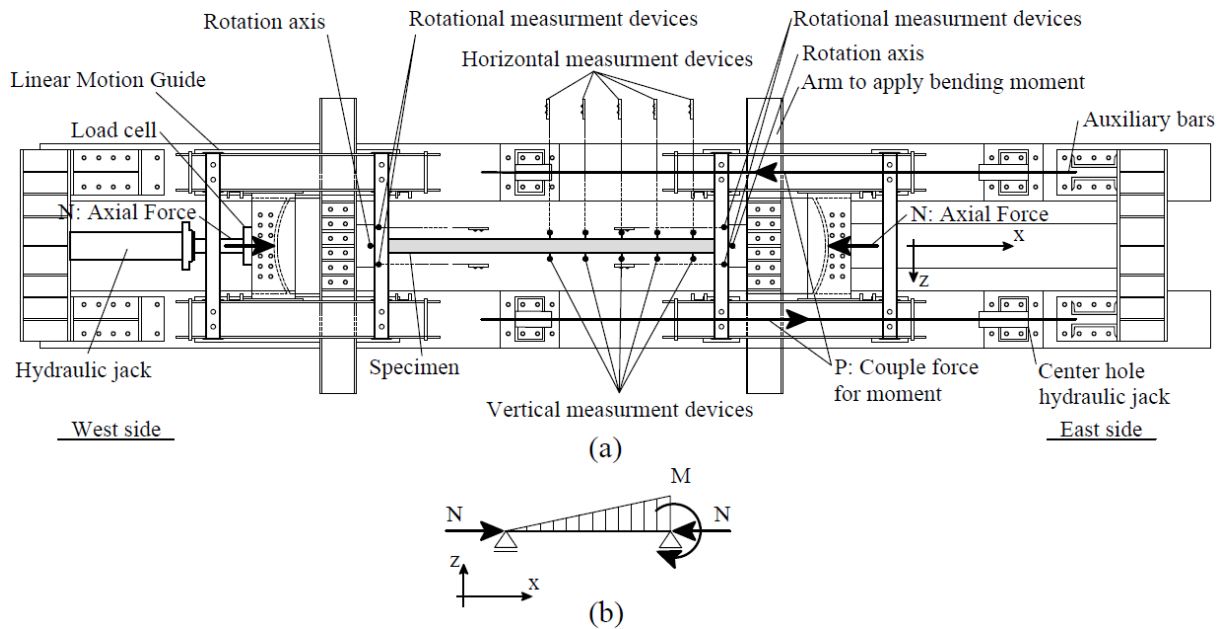


Figure 2. Experimental test from Kazuya [18]: (a) plan view and (b) boundary condition. Adapted from [18]

Since the aim of this paper was to present a lumped damage model for analysing local buckling in steel SHS and RHS, only Kazuya's experimental results [18] with collapse mode determined by local buckling (LB) and geometric nonlinearity along with local buckling (GN + LB) were numerically analysed. Table 2 presents the analysed experimental results. The numbers following the terms "B", "bt", "ny", and "L" in the specimen's name indicate, respectively, the nominal width of the cross-section, nominal width-thickness ratio, axial force ratio ( $N/N_y$ ), and length of the specimen, being  $N_y$  the yield axial force. Additionally, Tab. 2 provides information on the applied axial load ( $N$ ), the maximum experimental bending moment ( $M_{\max}^{\text{exp}}$ ), the corresponding rotation at the maximum bending moment ( $\theta_{\max}^{\text{exp}}$ ) and the collapse mode of the specimen.

Table 2. Experimental results from Kazuya [18]

No.	Specimen's name	$L$ (mm)	$n_y = \frac{N}{N_y}$	$N$ (kN)	$M_{\max}^{\text{exp}}$ (kN.m)	$\theta_{\max}^{\text{exp}}$ (rad)	Collapse mode
1	B125bt21ny30L1800	1800	0.30	329.0	52.73	0.0891	LB
2	B125bt21ny40L1800	1800	0.40	438.7	45.41	0.0750	GN + LB
5	B125bt21ny20L2100	2100	0.20	219.4	56.58	0.1133	LB
6	B125bt21ny30L2100	2100	0.30	329.0	50.87	0.0935	GN + LB
9	B125bt21ny20L2400	2400	0.20	219.4	54.20	0.1198	LB
14	B150bt17ny20L2900	2900	0.20	366.4	102.3	0.1210	GN + LB

According to Kazuya [18], in the specimens where the collapse mode was determined by GN + LB, local buckling was observed near the position  $x = 0.80L$ . Thus, to adequately capture the behaviour of this collapse mode, the finite element mesh was discretized into two elements, with an intermediate node strategically positioned at  $x = 0.80L$ . Additionally, convergence tests were performed for the parameters  $\beta$  of the yield function and  $k_m$  of the damage evolution law, where the best numerical results were obtained with values of 100 and 5, respectively.

Figure 3 presents the comparison between numerical results and Kazuya's experiments [18]. The numerical models satisfactorily reproduced the trend observed in experimental curves, adequately representing the elastic and elastic-plastic behaviours. Additionally, the numerical models demonstrated the capability of capture geometric nonlinearity. However, despite the satisfactory approximation after local buckling, the numerical models were unable to describe the nonlinear behaviour of stiffness degradation due to the linear consideration of the damage evolution law.

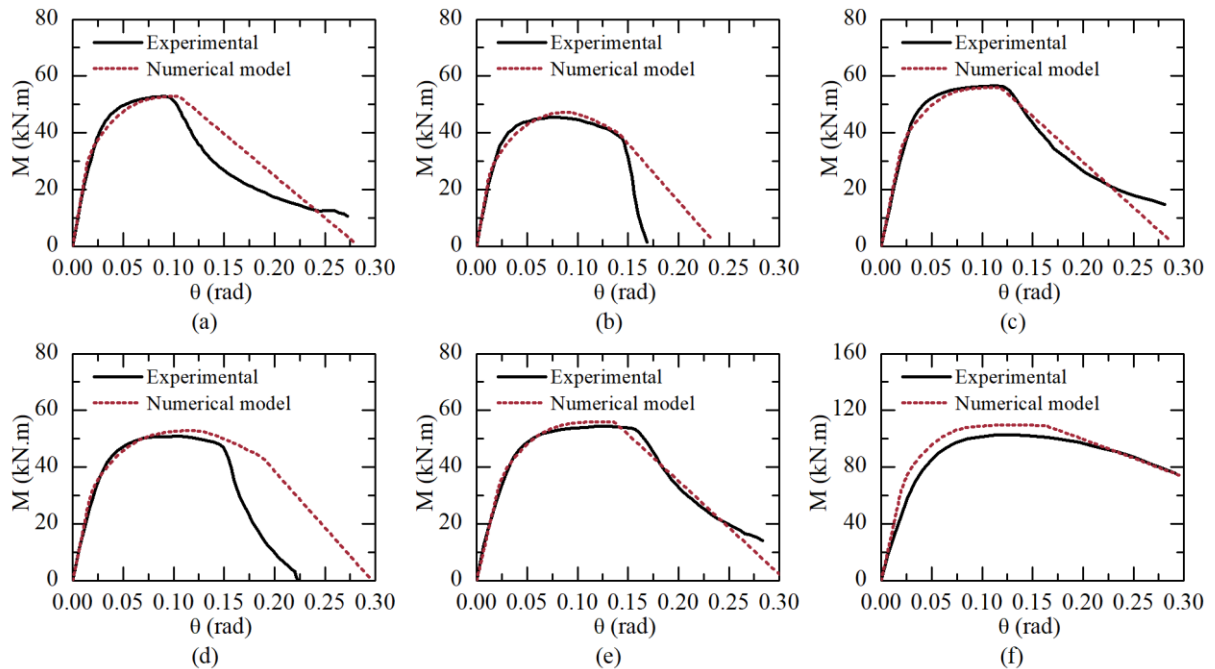


Figure 3. Experimental [18] and numerical  $M$  vs.  $\theta$  curves of SHS: (a) No. 1, (b) No. 2, (c) No. 5, (d) No. 6, (e) No. 9 and (f) No. 14 (see Tab. 2)

## 4 Conclusions

The numerical results indicated that the model satisfactorily captures the behaviour observed in the experimental curves. However, experiments exhibit a characteristic nonlinear curve after the onset of local

buckling. Thus, due to the linear consideration of the damage evolution law, the numerical models were unable to accurately describe this behaviour.

Therefore, it is recommended for future work to propose a nonlinear damage evolution law, aiming to improve the numerical response of the model and more adequately reproduce the structural behaviour.

**Acknowledgements.** The first author acknowledges CAPES (*Coordenação de Aperfeiçoamento de Pessoal de Nível Superior*) for the financial support of his D.Sc. studies. The authors acknowledge the Post-Graduate Programme in Civil Engineering of the Federal University of Alagoas (PPGEC/UFAL) for the English proofreading sponsorship.

**Authorship statement.** The authors hereby confirm that they are the sole liable persons responsible for the authorship of this work, and that all material that has been herein included as part of the present paper is either the property (and authorship) of the authors, or has the permission of the owners to be included here.

## References

- [1] C.-C. Ou, J. Iyama, Y. Fukushima, F. He, T. Hasegawa and S. Hiroshima. "Post-earthquake damage detection of local buckling in rectangular hollow section columns based on local stiffness calculated by strain response". *Engineering Structures*, vol. 292, pp. 116485, 2023.
- [2] Y. Shen and R. Chacón. "Flexural stiffness reduction for stainless steel SHS and RHS members prone to local buckling". *Thin-Walled Structures*, vol. 155, pp. 106939, 2020.
- [3] L. Yang, F. Yin, J. Wang, A. Bilal, A. H. Ahmed and M. Lin. "Local buckling resistances of cold-formed high-strength steel SHS and RHS with varying corner radius". *Thin-Walled Structures*, vol. 172, pp. 108909, 2022.
- [4] C. Quan and M. Kucukler. "Simulation and cross-section resistance of stainless steel SHS and RHS at elevated temperatures". *Thin-Walled Structures*, vol. 189, pp. 110849, 2023.
- [5] J.-L. Ma, M. Pandey, T.-M. Chan and B. Young. "Design of cold-formed high strength steel square and rectangular hollow section beam-columns". *Thin-Walled Structures*, vol. 185, pp. 110483, 2023.
- [6] P. Pannuzzo, S. Chen and T.-M. Chan. "Experimental investigation on cold-formed steel hollow sections with moderate heat treatment under combined compression and cyclic lateral loads". *Journal of Constructional Steel Research*, vol. 216, pp. 108609, 2024.
- [7] J. A. V. Bazán, A. T. Beck and J. Flórez-López. "Random fatigue of plane frames via lumped damage mechanics". *Engineering Structures*, vol. 182, pp. 301-315, 2019.
- [8] R. M. Bosse, J. Flórez-López, G. M. S. Gidrão, I. D. Rodrigues and A. T. Beck. "Collapse mechanisms and fragility curves based on Lumped Damage Mechanics for RC frames subjected to earthquakes". *Engineering Structures*, vol. 311, pp. 118115, 2024.
- [9] P. Inghlessis, G. Gómez, G. Quintero and J. Flórez-López. "Model of damage for steel frame members". *Engineering Structures*, vol. 21, n. 10, pp. 954-964, 1999.
- [10] P. Inghlessis, S. Medina, A. López, R. Febres and J. Flórez-López. "Modeling of local buckling in tubular steel frames by using plastic hinges with damage". *Steel and Composite Structures*, vol. 2, n. 1, pp. 21-34, 2002.
- [11] R. Febres, P. Inghlessis and J. Flórez-López. "Modeling of local buckling in tubular steel frames subjected to cyclic loading". *Computers & Structures*, vol. 81, n. 22-23, pp. 2237-2247, 2003.
- [12] N. Guerrero, M. E. Marante, R. Picón and J. Flórez-López. "Model of local buckling in steel hollow structural elements subjected to biaxial bending". *Journal of Constructional Steel Research*, vol. 63, n. 6, pp. 779-790, 2007.
- [13] L. A. B. Silva, H. S. D. Argôlo and D. L. N. F. Amorim. "Lumped damage model Applied to local buckling in steel rectangular hollow section subjected to compressive axial force with bending moment". *International Journal of Steel Structures*, vol. 22, n. 1, pp. 319-332, 2022.
- [14] G. H. Powell. "Theory of nonlinear elastic structures". *Journal of the Structural Division ASCE*, vol. 95, n. 12, pp. 2687-2701, 1969.
- [15] J. Flórez-López, M. E. Marante and R. Picón. *Fracture and damage mechanics for structural engineering of frames: state-of-the-art industrial applications*. IGI Global, 2015.
- [16] J. Lemaitre. *A Course on Damage Mechanics*. Springer-Verlag, 1996.
- [17] S. Yamada, T. Ishida and Y. Jiao. "Hysteretic behavior of RHS columns under random cyclic loading considering local buckling". *International Journal of Steel Structures*, vol. 18, n. 5, pp. 1761-1771, 2018.
- [18] M. Kazuyua. *Study on elasto-plastic behavior of square steel tubular column under compressive axial force with bending moment*. PhD thesis, Nagoya Institute of Technology, 2017. (in Japanese).
- [19] ANSI/AISC, "ANSI/AISC 360-22, Specification for structural steel buildings", American Institute of Steel Construction (AISC), 2022.
- [20] K. Tayyebi, M. Sun, K. Karimi, R. Daxon and B. Rossi. "Experimental investigation of direct-formed square and rectangular hollow section beams". *Journal of Constructional Steel Research*, vol. 186, pp. 106898, 2021.